HYDROPHILIC *VERSUS* HYDROPHOBIC OLEATE COATED MAGNETIC PARTICLES

E. PUSCASU[1], L. SACARESCU[2], A. DOMOCOS[1], C. LEOSTEAN[3], R. TURCU[3], D. CREANGA[1], M. BALASOIU[4,5]

[1]"Alexandru Ioan Cuza" University, Physics Faculty, Iasi, Romania
[2]"Petru Poni" Institute of Macromolecular Chemistry, Iasi, Romania
[3]National Institute of Research and Development of Isotopic and Molecular Technology, Cluj, Romania
[4]Institute of Nuclear Research, Dubna, Russian Federation
[5]"Horia Hulubei Institute of Physics and Nuclear Engineering, Bucharest, Romania
Corresponding author: dorina.creanga@gmail.com

Received August 31, 2015

Oleic acid was used to develop hydrophobic coating shell for magnetic nanoparticles (MNPs) stabilization in hydrophobic medium; sodium oleate was used to yield hydrophilic coating of MNPs in colloidal aqueous suspension. Microstructural and magnetic properties were investigated by standard methods. The interpretation of the observed microstructural and magnetic features was based on the differences in coating shell arrangement, *i.e.* single oleate layer in hydrophobic colloidal MNPs compared to double oleate layer in hydrophilic MNP sample. In this latter case coated particle interaction seems to be favored resulting in some clusters with character of mass fractals (2.4 fractal dimension) as shown from SAXS data analysis.

Key words: iron oxides, oleate ions, magnetic colloids.

PACS: 75.50. Mm, 75.75.Cd, 81.07-b

1. INTRODUCTION

Previous literature reports on magnetic nanoparticle yielding in the form of uniform and stable suspensions in various liquids, by applying versatile co-precipitation method, suggested that oleate ion is able to develop one of the strongest interactions with iron ions at the surface of iron oxide nanoparticles under controlled conditions of temperature, concentration, pH, stirring duration and washing steps of intermediate ferrophase and/or of magnetic colloid.

In the early decades of ferrofluids, intended mainly for technical uses, carrier fluids were chosen as various hydrocarbons either pure reagents (toluene, benzene [1, 2] or technical mixtures – transformer oil, kerosene [3, 4]). Two step chemical route was largely applied providing first coprecipitated ferric and ferrous mixed oxides in alkaline medium that were let then to react with oleic acid at high temperature under vigorous stirring to favor chemical interaction of iron ions with side carboxyl groups from oleate long chain. Peer control of iron precursor salt stoichiometry, pH adjustment and oleic acid amount tuning could ensure oleate monolayer around MNPs functioning as steric stabilizer in hydrophobic dispersion liquids.

Biological and medical implementation of colloidal MNPs required ferrophase surface modification aiming to confer it hydrophilic properties for homogeneous and stable dispersion in water. Among various hydrophilic and biocompatible molecules that were found able to bind to metal ions exposed at the MNP surface, sodium oleate was preferred in many cases due to its long chain - very convenient for steric stabilization of colloidal suspension against magnetic dipole attraction forces. Under controlled reaction parameters, coprecipitation method allowed oleate ions arranging in double layer around MNPs that leads finally to hydrophilic properties of colloidal magnetic systems. While the first oleate shell results from chemical interaction at the level of carboxylic terminal groups with MNP metal ions, the second oleate shell is formed by steric coupling between oleate-oleate hydrophobic chains so that the hydrophilic carboxyl terminals of second layer remain exposed to the water environment [5, 6, 7]. Also biocompatible features of sodium oleate were demonstrated [8] as well as the availability of its exposed carboxyl groups to attach biocompatible polymers [9] and further drugs or biomolecules of therapeutic interest [10].

2. EXPERIMENTAL

2.1. SYNTHESIS TECHNOLOGY

$FeCl_2 \times 4H_2O$, $FeCl_3 \times 6H_2O$, NaOH, $C_{18}H_{34}O_2$, $C_{18}H_{33}NaO$, HCl, n-hexane and kerosene chemicals used in experiments were analytical high purity reagents purchased from Sigma-Aldrich, Lach-ner, Merck that were used without further purification, while all solutions and aqueous suspension were made with deionized water (18.2 MΩ/cm, Barnstead ultrapure water system). Magnetic nanoparticles were synthesized through chemical co-precipitation method described by Massart [11] and modified as follows. In a flat bottom flask equipped with thermal heating and magnetic stirring bar were placed 300 mL aqueous solution of 134 mM ferric chloride and 300 mL aqueous solution of 67 mM ferrous chloride. 150 mL aqueous solution of 2 M sodium hydroxide was added dropwise over ferric salts mixture

under continuous mixing at 80 °C; next, the black precipitate was washed with deionized water to remove all impurities and dried overnight in vacuum conditions at 60 °C. 3 mL oleic acid (1:6 oleic acid / n-hexane) was added on dry powder of black precipitate with constant mechanical stirring to ensure MNPs stabilization; after hexane evaporation 35 mL of kerosene were added under continuous stirring. Finally, 20 mL of stable magnetic nanoparticles coated with mono layer of oleate in non-polar medium was obtained (sample P1). In similar conditions of temperature and stirring speed, but using 1.7 M aqueous solution of sodium hydroxide for same amounts of precursor salts, the black precipitate was obtained and was washed with acidic deionized water to remove all impurities; 3g sodium oleate dissolved in deionized water was added over wet powder under constant mechanical stirring for 1h to ensure MNPs stabilization in aqueous suspension (Fig. 1).

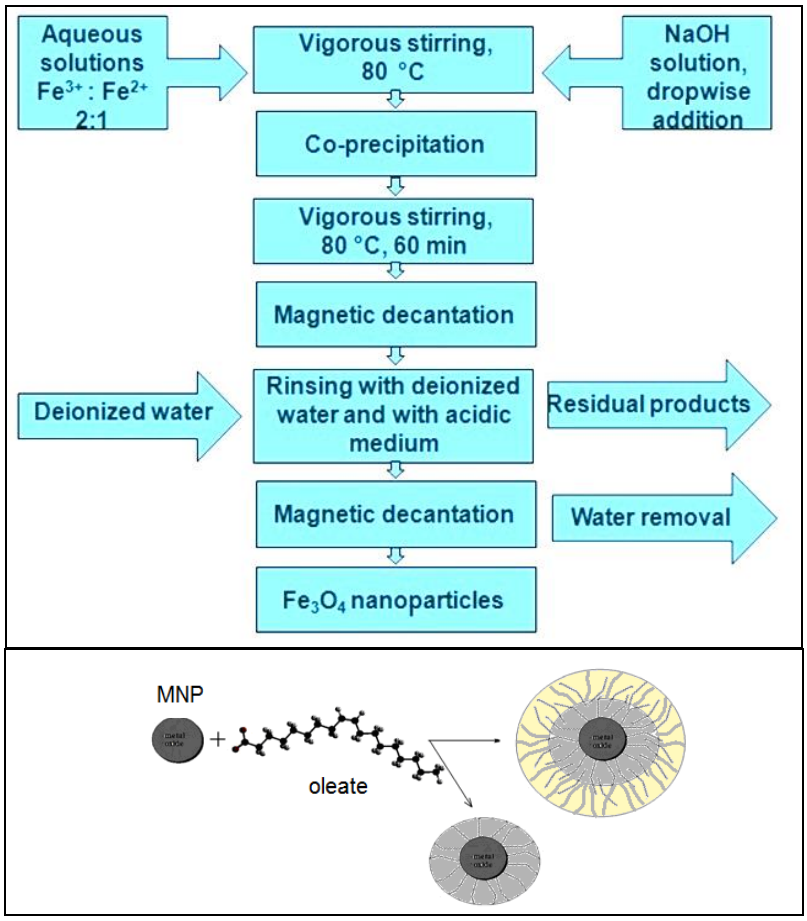

Fig. 1 – Preparation steps of magnetic nanoparticles stable suspension.

Finally, 35 mL of stable magnetic nanoparticles coated with hydrophilic oleate layer in polar medium was obtained (sample P2).

2.2. INVESTIGATION METHODS

Transmission Electron Microscope (TEM) model Hitachi High-Tech HT7700 was utilized to image and measure MNP physical diameter.

X-ray Diffraction (XRD) analysis using Shimadzu LabX XRD-6000 diffractometer (Cu-Kα radiation at $\lambda = 1.5406$ Å) was utilized for checking crystalline structure of ferrophase.

Small-Angle X-Ray Scattering experiments (SAXS) was carried out by Nanostar U-Bruker system (Vantec 2000 detector, X-ray I μS microsource); the samples were sealed in a quartz capillary and measured under vacuum at constant temperature (25 °C) for 10000 s.

Magnetic properties analysis (VSM) was performed by MicroMag model 2900/3900 at room temperature in order to evidence magnetization capacity of nanoparticles up to 5T and to estimate magnetic diameter of MNPs.

3. RESULTS AND DISCUSSIONS

TEM investigation results showed generally round aspect particles that could be quasi-spherical as well as thick cylinders (Fig. 2). Most frequent size was of around 8.5 nm for P1 sample and respectively of 11.5 nm for P2 sample – as resulted from over 1000 individual measurements approximating theoretical size range of MNP suspension stability [12]; apparently, sample P2 showed an agglomeration tendency of nanoparticles on dried suspension sample.

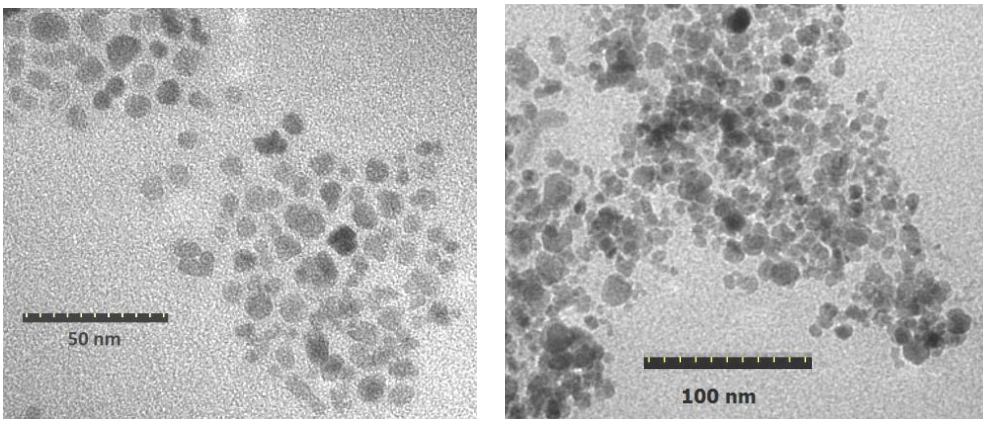

Fig. 2 – TEM image of MNP samples (P1 – left and P2 – right).

Crystallinity properties were evidenced by XRD (Fig. 3). Analysis of raw XRD data confirmed spinel structured crystallites; possible partial conversion to maghemite at the surface of some magnetite nanoparticles could occur during open air manipulation (Table 1). However peak positions have quite similarly positions so that one should admit that both iron oxides coexists in the analyzed MNPs. Average size of the crystalline domains D_{ijk} can be approximated from Scherrer's equation applied on raw data:

$$D_{ijk} = \frac{K \cdot \lambda}{\beta \cdot \cos\theta} \tag{1}$$

where K is a dimensionless factor which varies with the shape of the crystallite (in this case K= 0.89), λ (Å) is X-ray wavelength, β (rad) is line broadening at half the maximum intensity and θ (rad) is the Bragg angle of (ijk) peak. Thus, average size of the crystalline domains for sample P1 and P2 were found to be $D_{ijk\text{-}P1}$= 8.6 nm and respectively $D_{ijk\text{-}P2}$= 10.1 nm resulted from averaging of strongest peaks which occurred between 20 and 80 degrees (Table 1).

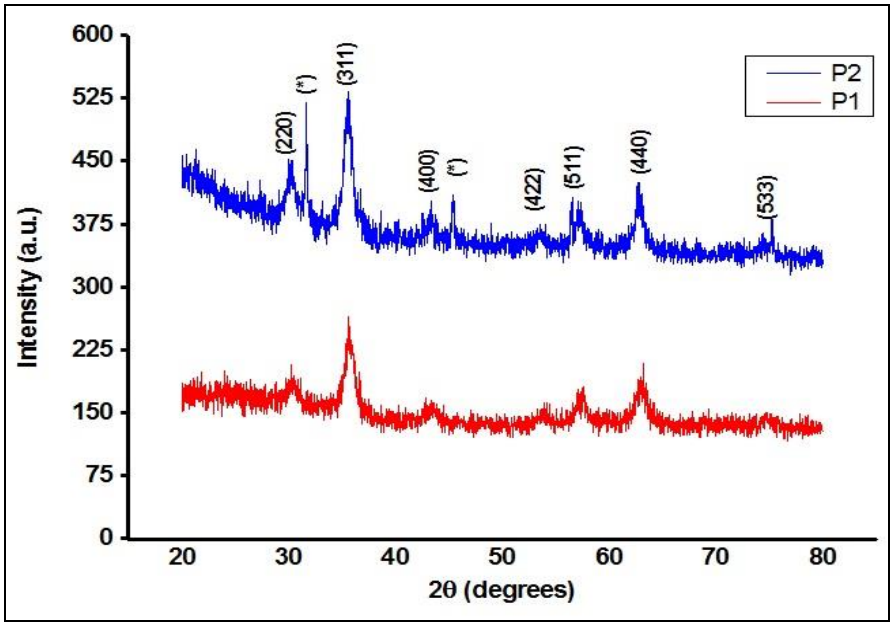

Fig. 3 – XRD recordings for P1 and P2.

(*) marks peaks due either to zero-valent iron [13] or/and associated to sodium [14] for double oleate coating of MNPs. Similar results were reported by Lopez *et al.* [15].

Table 1

Estimation of (ijk) peak position and crystallite size from XRD raw data

Miller indices	**2θ (°)**		**β (rad)**		**D_{ijk} (nm)**	
	P1	P2	P1	P2	P1	P2
(220)	30.20	30.28	0.01918	0.01430	7.4	9.9
(*)	–	31.68	–	–	–	–
(311)	35.60	35.60	0.01849	0.01186	7.8	12.1
(400)	43.38	43.38	0.01326	0.01256	11.1	11.7
(*)	–	45.38	–	–	–	–
(422)	53.96	53.60	0.01744	0.01465	8.8	10.5
(511)	57.54	57.10	0.01779	0.01953	8.8	7.9
(440)	62.98	62.90	0.02128	0.01866	7.6	8.6

SAXS investigation method has led to the next results (Fig. 4).

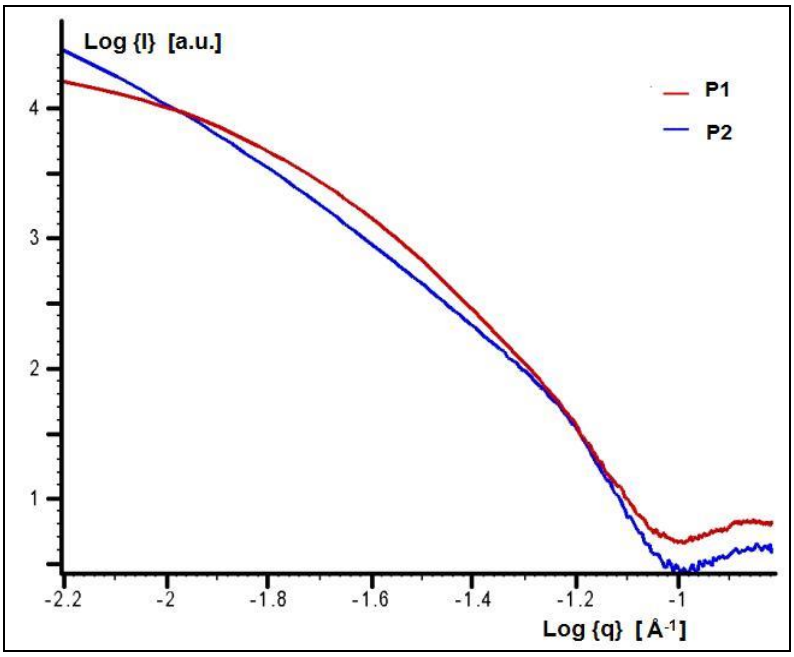

Fig. 4 – SAXS data analysis (*I* – intensity; *q* – scattering vector).

Thus, in the case of the P1 sample the scattering curve has the characteristic profile for round shape very small particles [16].

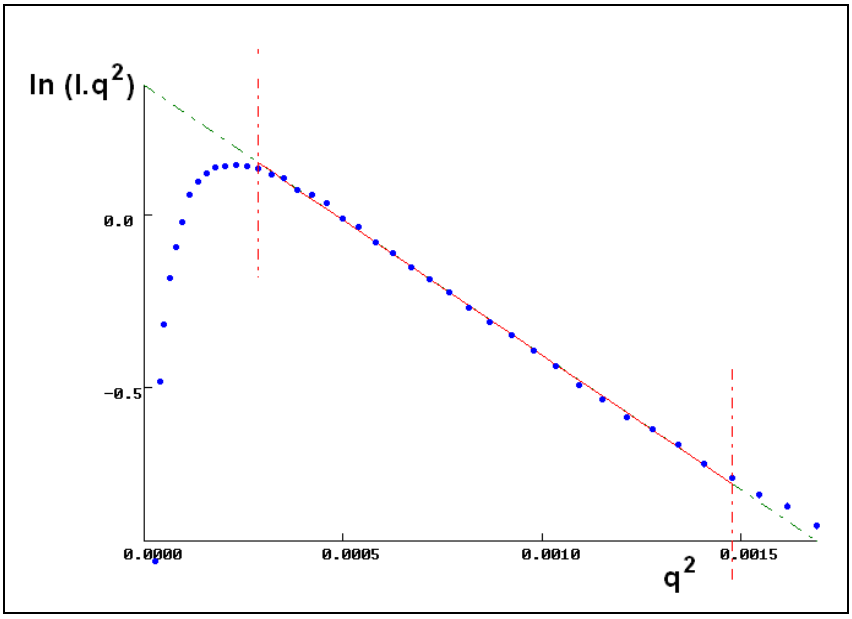

Fig. 5 – Guinier fit for sample P1 using the flat particle approximation.

An estimation of the average dimension for these particles was obtained by calculating the radius of gyration using the Guinier plot for flat particles (Fig. 5):

$$I = I_0 \exp(-q^2 R_g^2)/q^2 \tag{2}$$

where I_0 represents the scattering intensity for $q = 0$. The plotting of $\ln(q^2 I)$ *versus* q^2 for small q should yield a strait line according to equation (3):

$$\ln(q^2 I) = \ln(I_0) - q^2 R_g^2 \tag{3}$$

Thus, the slope of the linear region can be used to calculate R_g. The gyration radius calculated by this method is: R_g = 2. 61 nm.
In real space the relation allowing calculation for the radius of an infinitely thin disk, R, is:

$$R^2 = 2R_g^2; R = 1.41R_g \tag{4}$$

Thus, the averaged maximal dimension of the platelets, D_{max}, is: D_{max} = 2 (1.41 R_g) = = 2.82 R_g = 7.3 nm. In conclusion the SAXS analysis shows that the MNP particles in the sample are highly dispersed and polydisperse. The shape of the particles is close to that of thin discs having an average maximal dimension centered at 7.3 nm. This dimension is in good agreement with the TEM analysis results. In the

case of the sample P2 a linear area one can see, in the linear region of small q values, profile characteristic of fractal geometry structures.

The interpretation of the scattering effects on such complex poly-dispersed systems, considerably simplifies in case in which the fractal geometry theory is applied. In SAXS experiments, signal strength scattered of the fractal objects can be described by a simple relationship (5):

$$I(q) = I_0 q^{-\alpha}, \tag{5}$$

where I_0 is a constant [17, 18, 19]. The value of the exponent, α, can be calculated from log/log representation. Based on it one can then determine the mass fractal dimension (D_m) and / or area (D_s).

For the calculation of mass fractal: $\alpha = D_m$; and $1 < \alpha < 3$; for the calculation of fractal surface: $\alpha = 6\text{-}D_s$ while $3 < \alpha < 4$ because $2 < D_s < 3$. P2 Sample shows linear region in the small q area (curve slope in this area is $\alpha = 2.4$), it is characteristic for presence of mass fractal with discoid clusters assembled from small particles. The Guinier plot for sample P2 (the same approach as in P1 case) was used to obtain R_g (Fig. 6).

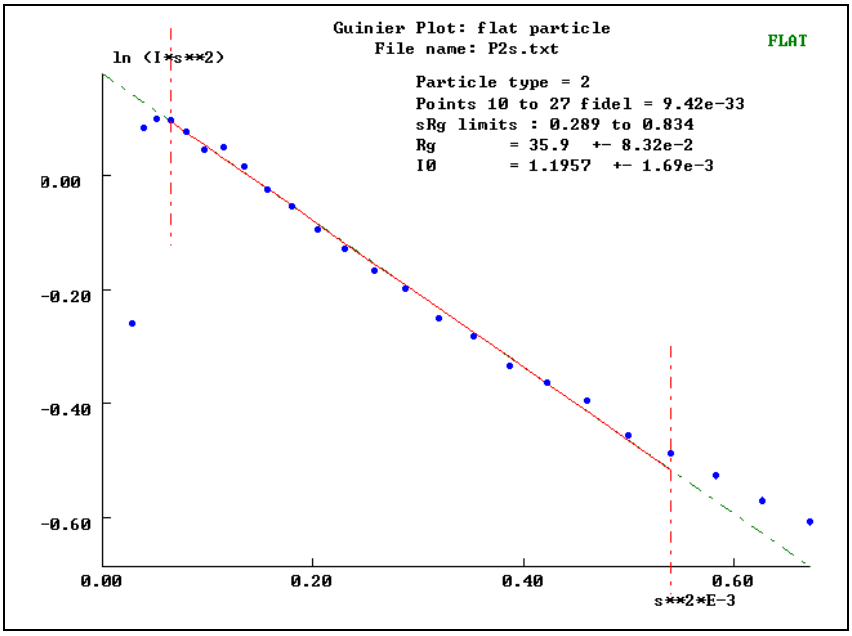

Fig. 6 – Guinier fit for sample P2 using the flat particle approximation.

The best fit corresponds to the flat particle model. Therefore, in the real space $D_{max} = 2\ (1.41\ R_g) = 2 \times 1.41 \times 3.5 = 9.87$ nm.

Magnetic properties analyses were estimated from the magnetization curve (Fig. 7) while saturation magnetization and magnetic diameter are presented in Table 2.

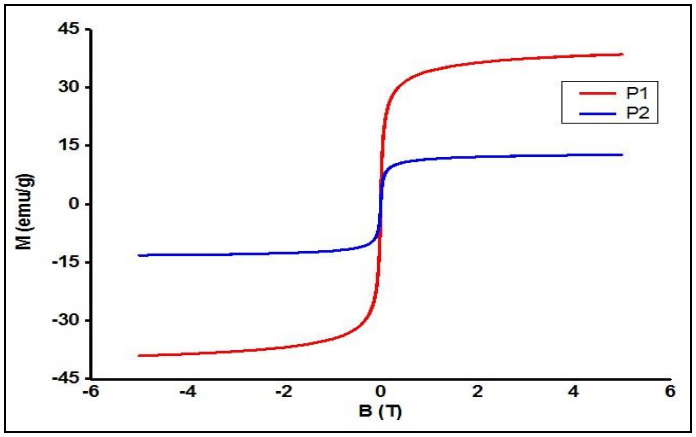

Fig. 7 – Magnetization curves for P1 and P2.

Magnetic diameter was calculated from Langevin's theory (eq. (6)):

$$d_M^3 = \frac{18k_BT}{\pi\mu_0 M_s \cdot m_s}\left(\frac{dM}{dH}\right)_{H\to 0} \tag{6}$$

where d_M is MNP magnetic diameter, k_B is Boltzmann's constant, T is the absolute temperature, M_s is saturation magnetization of MNP coated powder, μ_0 is vacuum magnetic permeability, $m_s = 0.48\cdot 10^6$A/m (bulk magnetite saturation magnetization [20] and (dM/dH) is the slope in the graph origin (for H – magnetic field intensity – near zero).

Table 2

Microstructural and magnetic properties of the MNP samples

Sample	Maximum magnetization at 5T (emu/g)	Magnetic diameter (nm)	Physical diameter (nm)	XRD size (nm)	SAXS size (nm)
P1	38.8	7.89	8.5	8.6	7.3
P2	12.9	8.29	11.5	10.1	9.87

The magnetometry results are in concordance with [2] where the authors reported also higher saturation magnetization for hydrophobic oleate/MNPs than for hydrophilic ones**.**

Various studies as those mentioned in the introductory part indicate that sodium oleate could be considered as efficient stabilizer of magnetite nanoparticles (MNPs) in aqueous suspensions due to its hydrophilic properties which recommend the final product for applications in biology and medicine. Some authors [21] reported monodisperse oleate/magnetite MNPs yielding for tumor thermo therapy; they evidenced crystallite average size of around 9.8 nm in concordance with average physical diameter revealed by TEM imaging (10.1 nm) while for magnetic cores around 8 nm average value was estimated from Langevin's theory application. As general observation the non-magnetic shell of hydrophilic colloidal MNPs is thicker than that of hydrophobic colloidal MNPs. Thus one may assume [22] that – when synthesized in quite similar conditions – the maximum diameter of colloidal MNPs dispersed in aqueous suspensions is higher than for MNPs dispersed in hydrocarbons.

4. CONCLUSIONS

Magnetic nanosystems were prepared from iron oxide cores coated with long chain molecular shell to ensure stability in suspensions for applications in technical and life sciences. By providing oleate ions from oleic acid mono-layer hydrophobic coating shell was yielded and colloidal MNPs dispersed in hydrocarbons. Oleate supplying from sodium oleate resulted in double layered MNPs with hydrophilic properties for dispersion in aqueous media and further utilization in biomedical procedures. Good granularity (all estimated particle size were no larger than 11 nm) and superparamagnetic properties were evidenced in both magnetic colloidal samples. Further study is needed to improve technological preparation based on the versatility of coprecipitation method while deeper investigation of MNP structure is planned to estimate the weight of ferric and ferrous ions in the resulted mixed oxides.

Acknowledgements. This research was supported by IUCN-UAIC JINR grant 57/04-4-1121-2015.

REFERENCES

1. D. Bica, Rom. Rep. Phys. **47**, 265-272 (1995).
2. M.T. López-López, J.D.G. Durán, A.V. Delgado, F. González-Caballero, J. Colloid. Interface. Sci. **291**, 144-151 (2005).
3. L.A. Akselrod, G.P. Gordeev, G.M. Drabkin, I.M. Lazebnik, V.T. Lebedev, JETP **91**, 531 (1986).
4. M.V. Avdeev, M. Balasoiu, V.L. Aksenov, V.M. Garamus, J. Kohlbrecher, D. Bica, L. Vekas, J. Magn. Magn. Mater. **270**, 371-379 (2004).
5. A. Tomitaka, K.Ueda, T. Yamada, Y. Takemura, J. Magn. Magn. Mater. **324**, 3437-3442 (2012).
6. K. Yang, H. Peng, Y. Wen, N. Li, Appl. Surf. Sci. **256**, 3093–3097 (2010).

7. E. Tombácz, D.Bica, A.Hajdú, E.Illés, A.Majzik, L.Vékás, J. Phys. Condens. Matt. **20**, 204103 (2008).
8. J. Sun, S. Zhou, P. Hou, Y. Yang, J. Weng, X. Li, M. Li, J. Biomed. Mater. Res. **80A**, 333–341 (2007).
9. M. Koneracká , V. Závišová, M. Timko, P. Kopčanský, N. Tomašovičová, K. Csach, Acta Phys. Pol. A, **113**, 595-598 (2008).
10. A. Juríková, K. Csach, J. Miškuf, M. Koneracká, V. Závišová, P. Kopčanský, Acta Phys. Pol. A **118**, 990-992 (2010).
11. R. Massart, IEEE Trans. Magn. **17**, 1247-1248 (1981).
12. R.E. Rosensweig, *Ferrohydrodynamics*, Cambridge University Press (1985).
13. K.S. Lin, N.B. Chang, T.D. Chuang, Sci. Technol. Adv. Mater. **9**, 0205015 (2008).
14. J. Chen, Y. Wang, X. Ding, Y. Huang, K. Xu, Anal. Meth. **6**, 8358-8367 (2014).
15. J.A. Lopez, F. González, F.A. Bonilla, G. Zambrano, M.E. Gómez, Rev. Latinoam. Metal. Mater., **30**, 60-66 (2010).
16. O. Glatter, O. Kratky, *Small Angle X-Ray Scattering*, Academic Press (1982).
17. E. Martin, A.J. Hurd, J. Appl. Cryst. **20**, 61-78 (1987).
18. P.W. Schmidt; J. Appl. Cryst. **24**, 414-435 (1991).
19. J. Teixeira; J. Appl. Cryst. **21**, 781-785 (1988).
20. A. Layek, Pandey, A. Pandey, H.C. Verma, Int. J. Eng. Sci. Technol. **2**, 33-39 (2010).
21. R.P. Araújo-Neto, E.L. Silva-Freitas, J.F. Carvalho, T.R.F. Pontes, K.L. Silva, I.H.M. Damasceno, E.S.T. Egito, A.L. Dantas, M.A. Morales, A.S. Carriço, J. Magn. Magn. Mater. **364**, 72–79 (2014).
22. B. Jeyadevan, I. Nakatani, H. Oka, K. Tohji, Braz. J. Phys. **31**, 347-349 (2001).